Inorganic Chemistry

Article

pubs.acs.org/IC

# Probing the Protonation State and the Redox-Active Sites of Pendant Base Iron(II) and Zinc(II) Pyridinediimine Complexes

Mayra Delgado,[†] Samantha K. Sommer,[†] Seth P. Swanson,[†] Robert F. Berger,[†] Takele Seda,[‡] Lev N. Zakharov,[§] and John D. Gilbertson*[,†]

[†]Department of Chemistry, and [‡]Department of Physics, Western Washington University, Bellingham, Washington 98225, United States

[§]Department of Chemistry, University of Oregon, Eugene, Oregon 97403, United States

Supporting Information

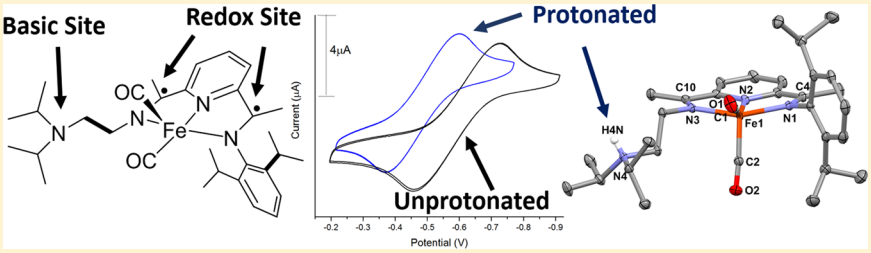


**ABSTRACT:** Utilizing the pyridinediimine ligand [(2,6-$^{i}$PrC$_6$H$_3$)N═CMe)(N($^{i}$Pr)$_2$C$_2$H$_4$)N═CMe)C$_5$H$_3$N] (didpa), the zinc(II) and iron(II) complexes Zn(didpa)Cl$_2$ (**1**), Fe(didpa)Cl$_2$ (**2**), [Zn(Hdidpa)Cl$_2$][PF$_6$] (**3**), [Fe(Hdidpa)Cl$_2$][PF$_6$] (**4**), Zn(didpa)Br$_2$ (**5**), and [Zn(Hdidpa)Br$_2$][PF$_6$] (**6**), Fe(didpa)(CO)$_2$ (**7**), and [Fe(Hdidpa)(CO)$_2$][PF$_6$] (**8**) were synthesized and characterized. These complexes allowed for the study of the secondary coordination sphere pendant base and the redox-activity of the didpa ligand scaffold. The protonated didpa ligand is capable of forming metal halogen hydrogen bonds (MHHBs) in complexes **3**, **4**, and **6**. The solution behavior of the MHHBs was probed via p*K*a measurements and $^{1}$H NMR titrations of **3** and **6** with solvents of varying H-bond accepting strength. The H-bond strength in **3** and **6** was calculated *in silico* to be 5.9 and 4.9 kcal/mol, respectively. The relationship between the protonation state and the ligand-based redox activity was probed utilizing **7** and **8**, where the reduction potential of the didpa scaffold was found to shift by 105 mV upon protonation of the reduced ligand in Fe(didpa)(CO)$_2$.

## INTRODUCTION

Many metalloenzymes utilize noncovalent interactions such as hydrogen bonding (H-bonding) in the secondary coordination sphere to control reactivity at the primary coordination sphere.[1,2] Typically, these H-bonding interactions are utilized to regulate substrate orientation, tune the redox potential, and/or direct proton-transfer reactivity within the active site.[3,4] Hydrogen bonds or amino acid residues capable of H-bonding typically influence the electronics at the metal center during small molecule activation,[5] and this reactivity can be directed by well-positioned acidic/basic groups.[6,7] These so-called proton-responsive ligands are attractive features of many bioinspired complexes.[8−15]

In addition, many biological redox reactions occur by changing the protonation state at the enzyme active site.[16−18] These reactions are more formally referred to as "proton-coupled electron transfer" (PCET) reactions. In model systems where there is a formal separation between the redox and acid/base sites, the redox potentials are still pH dependent.[19,20] H-bonds are common in PCET between H$^+$ donors/acceptors, and the H-bonding properties of the system can dramatically affect the observed reactivity. In other words, reactions that involve *both* protons and electrons are ubiquitous in both chemistry and nature. Therefore, it is important to develop compounds and catalysts that can respond to the movement of *both* protons and electrons.[17] One example is the well-developed phosphine ligand system with pendant amine groups that have been shown to dramatically affect the electrocatalytic H$^+$ reduction/H$_2$ oxidation reaction(s).[21−24] In that system, the redox-active site is metal centered.

Given the utility of incorporating redox-activity into ligand scaffolds, the reactivity scope of numerous important processes has been expanded dramatically.[25−27] One consequence of this is that the ligand can be used to access redox states not available to the metal, opening new avenues of observed reactivity. In order to develop new methodologies involving the movement of *both* protons and electrons, we have been developing a series of iron(II) complexes based on the pyridinediimine (PDI) core which contain separated pendant bases (secondary sphere) and redox active sites within the ligand scaffold (Figure 1). Our initial studies revealed secondary coordination sphere H-bonding between Fe(II)-X (where X = Br$^-$ or OH$^-$) and the protonated pendant base (diisopropylamine) in the solid state[28]

**Received:** March 19, 2015
**Published:** July 23, 2015




DOI: 10.1021/acs.inorgchem.5b00633
*Inorg. Chem.* 2015, 54, 7239−7248

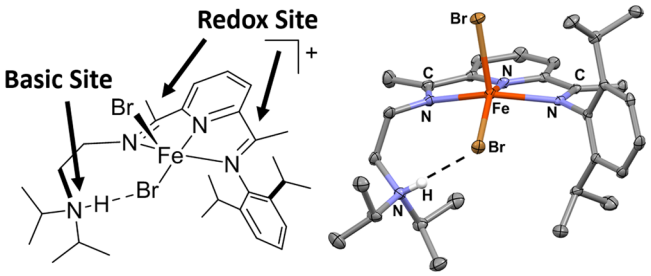


**Figure 1.** (Left) Chemdraw and (right) ORTEP diagrams of the previously reported Fe(didpa)$Br_2$ complex, highlighting secondary coordination sphere H-bonding as well as the separation of the basic sites and the ligand-based redox-active sites.

and that the secondary coordination sphere can be utilized to tune the reduction potential of the ligand-based redox-active sites.[29] Herein, we extend those studies to probe deeper into the role of the protonation state of the secondary coordination sphere and also the solution behavior of the secondary coordination sphere metal halogen hydrogen bonds (MHHBs). Given the intimate nature of the secondary coordination sphere protonation state and redox potentials in biological and catalytic systems, we also report the pH dependence of the potentials of the redox-active ligand in the reduced FePDI complexes.

## EXPERIMENTAL SECTION

**General Methods.** All reagents were purchased from commercial sources and used as received with the exception of *N,N*-(diisopropyl)-ethylenediamine, which was distilled immediately before use. The asymmetric PDI ligand [(ArN=C($CH_3$))$C_2H_3$N((=O)C($CH_3$)], and the didpa ligand, [(2,6-$^i$Pr−$C_6H_3$)N=CMe)(N-$^i$Pr-$NC_2H_4$)N=CMe)$C_5H_3$N] (Ar= 2,6-$^i$Pr−$C_6H_3$), were synthesized according to literature procedures.[28] Solvents were dried and deoxygenated with a PureSolv solvent purification system (CuO and alumina columns). Air sensitive materials were handled and stored on a Schlenk line or in a glovebox under $N_2$ atmosphere. Infrared spectra were recorded on a Thermo Scientific Nicolet iS10 FT-IR spectrometer equipped with an ATR accessory. $^1$H and $^{13}$C NMR spectra were recorded on a Unity Inova 500 MHz FT-NMR spectrometer. Data are reported in ppm from the solvent resonance as the internal standard unless otherwise noted. Solution magnetic susceptibilities were calculated from Evans method NMR measurements.[30] Solid-phase magnetic susceptibilities were recorded on a Johnson Matthey MSB-1 magnetic susceptibility balance that was calibrated with $HgCo(SCN)_4$. Diamagnetic correction factors were calculated from Pascal's constants.[31] Elemental analyses were performed by ALS (formerly Columbia Analytical Services) in Tuscon, AZ.

*Zn(didpa)$Cl_2$ (**1**).* A 250 mL round-bottomed flask was charged with the didpa ligand (2.00 g, 4.46 mmol), approximately 50 mL of $CH_2Cl_2$, $ZnCl_2$ (608 mg, 4.46 mmol), and a stir bar. The resulting yellow solution was stirred overnight forming a yellow solution with a yellow precipitate. The solid was isolated by vacuum filtration with a Buchner funnel using No. 2 filter paper, yielding a bright yellow solid in 95% yield (2.48 g, 4.24 mmol). FTIR (ATR): 1639, 1585 cm$^{-1}$ (C=N). $^1$H NMR (500 MHz, $CD_2Cl_2$) $\delta$ 8.39 (t, 1H), 8.18 (d, 2 H), 7.24 (s, 3H), 3.98 (t, 2H), 3.06 (m, 4H), 2.97 (m, 2H), 2.57 (s, 3H), 2.33 (s, 3H), 1.28 (d, 6H), 1.01 (m, 18H). $^{13}$C NMR (500 MHz, $CD_2Cl_2$) expected: 20; reported, 20; $\delta$ 15.3, 18.7, 20.6, 22.5, 22.9, 24.1, 24.6, 28.21, 44.9, 122.9, 123.8, 125.3, 125.6, 126.1, 138.9, 142.3, 143.4, 148.3, 149.7, 164.3 (C=N). UV−vis, $CH_2Cl_2$: 241 nm (16488 cm$^{-1}$ M$^{-1}$), 299 nm (5263 cm$^{-1}$ M$^{-1}$), 364 nm (939 cm$^{-1}$ M$^{-1}$). Anal. calcd for $C_{29}H_{44}Cl_2ZnN_4$: C, 59.54; H, 7.58, N, 9.58. Found: C, 59.79; H, 7.08; N, 9.55.

*Fe(didpa)$Cl_2$ (**2**).* A 20 mL scintillation vial was charged with the didpa ligand (0.400 g, 0.892 mmol), approximately 9 mL of $CH_2Cl_2$, 1 mL of THF, $FeCl_2$ (0.113 g, 0.892 mmol), and a stir bar. The blue solution was stirred overnight, forming a blue precipitate. The solvents were removed *in vacuo*, yielding a blue solid. The solid was redissolved with approximately 5 mL of $CH_2Cl_2$ and then filtered through Celite into a 20 mL scintillation vial. The filtrate was layered with pentane, and the vial was set aside for 1 day, after which blue crystals of **2** were isolated in 78% yield (0.400 g, 0.696 mmol). FTIR (ATR): 1620, 1582 cm$^{-1}$ (C=N). $^1$H NMR (500 MHz, $CD_2Cl_2$) $\delta$ −23.51 (s, 2H), −15.35 (s, 2H), −3.70 (s, 9H), −2.49 (s, 5H), −1.35 (s, 1H), 1.81 (s, 6H), 17.64 (s, 1H), 41.62 (s, 1H), 78.53 (s, 1H), 83.44 (s, 1H), 157.27 (s, 1H). $\mu_{eff}$: 5.8 $\mu_B$ (solid); 5.7 $\mu_B$ (solution). UV−vis, $CH_2Cl_2$: 294 nm (6847 cm$^{-1}$ M$^{-1}$), 679 nm (1788 cm$^{-1}$ M$^{-1}$). Anal. calcd for $C_{29}H_{44}Cl_2FeN_4$: C, 60.53; H, 7.71; N, 9.74. Found: C, 60.17; H, 7.77; N, 9.62.

*[Zn(Hdidpa)$Cl_2$][$PF_6$] (**3**).* A 20 mL scintillation vial was charged with **1** (0.100 g, 0.137 mmol), approximately 5 mL of $CH_2Cl_2$, and a stir bar. An additional 20 mL scintillation vial was charged with $NH_4PF_6$ (56.8 mg, 0.342 mmol), approximately 3 mL of dry $CH_3OH$, and a stir bar. After stirring for 10 min, the solution of $NH_4PF_6$ in $CH_3OH$ was transferred to the scintillation vial containing **1**. The resulting yellowish orange solution was stirred overnight. The solvents were removed *in vacuo*, yielding a yellowish orange solid. The solid was redissolved with approximately 5 mL of $CH_2Cl_2$. Any remaining solid was removed by filtering through a Celite plug, and the filtrate was added to a 20 mL scintillation vial. Ether was layered on top of the filtrate, and the vial was placed in a glovebox freezer for 48 h in order to crystallize the compound. The solid was isolated by vacuum filtration with a Buchner funnel using No. 2 filter paper, yielding a light yellow solid in 89% yield (0.089 g, 0.122 mmol). FTIR (ATR): 1642, 1586 cm$^{-1}$ (C=N); 832 cm$^{-1}$ ($PF_6^-$). $^1$H NMR (500 MHz, $CD_2Cl_2$) $\delta$ 8.60 (t, 1H), 8.50 (br s, 1H), 8.46 (d, 1H), 8.36 (d, 1H), 7.33 (m, 3H), 4.37 (t, 2H), 3.86 (sep, 2H), 3.74 (t, 2H), 2.90 (sep, 2H), 2.75 (s, 3H), 2.45 (s, 3H), 1.46 (m, 12 H), 1.30 (d, 6 H), 1.06 (d, 6 H). $^{13}$C NMR (500 MHz, $CD_3CN$) expected: 20; reported, 19; $\delta$ 15.3, 18.7, 23.7, 24.26, 28.1, 46.8, 47.0, 55.9, 97.3, 124.1, 126.7, 127.4, 128.0, 139.5, 144.4, 147.8, 148.6, 167.7 ($C_1$=$N_1$), 167.9 ($C_2$=$N_2$). UV−vis, $CH_2Cl_2$: 243 nm (17704 cm$^{-1}$ M$^{-1}$), 299 nm (7026 cm$^{-1}$ M$^{-1}$), 370 nm (520 cm$^{-1}$ M$^{-1}$). Anal. calcd for $C_{29}H_{45}Cl_2F_6ZnN_4P$: C, 47.65; H, 6.21; N, 7.67. Found: C, 47.25; H, 6.02; N, 7.64.

*[Fe(Hdidpa)$Cl_2$][$PF_6$] (**4**).* A 20 mL scintillation vial was charged with **2** (0.100 g, 0.174 mmol), approximately 5 mL of $CH_2Cl_2$, and a stir bar. In a separate 20 mL scintillation vial, $NH_4PF_6$ (56.7 mg, 0.348 mmol) was dissolved in approximately 3 mL of $CH_3OH$. The solution of $NH_4PF_6$ in $CH_3OH$ was transferred to the scintillation vial containing **1**. The dark purple solution was stirred overnight. The solvents were removed *in vacuo*. The resulting solid was redissolved in approximately 5 mL of $CH_2Cl_2$ and filtered through a Celite plug into a 20 mL scintillation vial. The filtrate was carefully layered with pentane and stored in a glovebox freezer for 24 h in order for the compound to crystallize (92% yield, 0.115 g, 0.160 mmol). FTIR (ATR): 1623, 1582 cm$^{-1}$ (C=N); 833 cm$^{-1}$ ($PF_6^-$). $^1$H NMR (500 MHz, $CD_2Cl_2$) $\delta$ −26.61 (s, 3 H), −3.72 (s, 6H), −2.76 (s, 1H), −1.8530 (s, 6H), 0.37 (s, 12H), 1.12 (s, 2H), 3.41 (s, 1H), 15.23 (s, 4H), 96.24 (s, 1H), 98.59 (s, 1H), 131.76 (s, 1H). $\mu_{eff}$: 4.8 $\mu_B$ (solid); 4.7 $\mu_B$ (solution). UV−vis, $CH_2Cl_2$: 297 nm (5755 cm$^{-1}$ M$^{-1}$), 601 nm (701 cm$^{-1}$ M$^{-1}$). Anal. calcd for $C_{29}H_{45}Cl_2F_6FeN_4P$: C, 48.28; H, 6.29; N, 7.77. Found: C, 47.03; H, 6.56; N, 7.47. The experimental and theoretical values deviate, possibly due to the solvent (pentane) present in the crystals (see X-ray section).

*Zn(didpa)$Br_2$ (**5**).* A 250 mL round-bottomed flask was charged with the didpa ligand (2.00 g, 4.46 mmol), approximately 50 mL of $CH_2Cl_2$, $ZnBr_2$ (1.00 g, 4.46 mmol), and a stir bar. The resulting yellow solution was stirred overnight forming a yellow solution with a yellow/orange precipitate. The solid was isolated by vacuum filtration with a Buchner funnel using No. 2 filter paper, yielding a yellow/orange solid in 88% yield (2.64 g, 3.92 mmol). FTIR (ATR): 1636, 1584 cm$^{-1}$ (C=N). $^1$H NMR (500 MHz, $CD_2Cl_2$) $\delta$ 8.43 (t, 1H), 8.21 (d, 2H), 7.26 (s, 3H), 4.07 (t, 2H), 3.01 (m, 6H), 2.63 (s, 3H), 2.37 (s, 3H), 1.30 (t, 6 H), 1.03 (d, 18 H). $^{13}$C NMR (500 MHz, $CD_2Cl_2$) expected: 20; reported, 20; $\delta$ 164.6 ($C_1$=$N_1$), 161.7 ($C_2$=$N_2$), 149.3,


DOI: 10.1021/acs.inorgchem.5b00633
*Inorg. Chem.* 2015, 54, 7239−7248

147.9, 143.7, 142.4, 138.9, 126.1, 125.9, 125.7, 123.8, 52.2, 49.1, 45.4, 28.4, 24.6, 24.5, 20.7, 19.2, 15.6. UV−vis, $CH_2Cl_2$: 299 nm (5306 $cm^{-1}$ $M^{-1}$), 376 nm (994 $cm^{-1}$ $M^{-1}$). Anal. calcd for $C_{29}H_{44}Br_2ZnN_4$: C, 51.69; H, 6.58; N, 8.31. Found: C, 52.05; H, 7.08; N, 8.03. The experimental and theoretical values deviate due to the solvent (ether) present in the crystals (see X-ray section).

*[Zn(Hdidpa)Br$_2$][PF$_6$] (**6**).* A 20 mL scintillation vial was charged with **5** (0.100 g, 0.122 mmol), approximately 5 mL of $CH_2Cl_2$, and a stir bar. An additional 20 mL scintillation vial was charged with $NH_4PF_6$ (40.0 mg, 0.245 mmol), approximately 3 mL of dry $CH_3OH$, and a stir bar. After stirring for 10 min, the solution of $NH_4PF_6$ in $CH_3OH$ was transferred to the scintillation vial containing **5**. The resulting yellowish orange solution was stirred overnight. The solvents were removed *in vacuo*, yielding a yellowish orange solid. The solid was redissolved with approximately 5 mL of $CH_2Cl_2$. Any remaining solid was removed by filtering through a Celite plug, and the filtrate was added to a 20 mL scintillation vial. Ether was layered on top of the filtrate, and the vial was placed in a glovebox freezer for 48 h in order to crystallize the compound. The crystals were isolated by vacuum filtration with a Buchner funnel using No. 2 filter paper, yielding a light yellow solid in 95% yield (0.0950 g, 0.116 mmol). FTIR (ATR): 1644, 1591 $cm^{-1}$ (C═N); 835 $cm^{-1}$ ($PF_6^-$). $^1$H NMR (500 MHz, $CD_2Cl_2$) $\delta$ 8.55 (t, 1H), 8.41 (d, 1H), 8.32 (d, 1H), 7.78 (br s, 1H) 7.28 (m, 3H), 4.37 (t, 2H), 3.83 (t, 2H), 3.71 (m, 2H), 2.90 (sep, 2H), 2.72 (s, 3 H), 2.42 (s, 3H), 1.40 (d, 12H), 1.28(d, 6H), 1.03 (d, 6H). $^{13}$C NMR (500 MHz, $CD_2Cl_2$) expected: 20; reported, 19; $\delta$ 167.3 ($C_1$═$N_1$), 166.6 ($C_2$═$N_2$), 148.8, 147.7, 144.6, 141.1, 139.3, 127.3, 127.1, 126.9, 124.2, 56.3, 47.4, 46.8, 28.5, 24.6, 19.3, 18.5, 17.2, 16.3. UV−vis, $CH_2Cl_2$: 301 nm (4818 $cm^{-1}$ $M^{-1}$), 365 nm (491 $cm^{-1}$ $M^{-1}$). Anal. calcd for $C_{29}H_{45}Br_2F_6ZnN_4P$: C, 42.49; H, 5.53; N, 6.83. Found: C, 42.25; H, 5.32; N, 6.97.

*Fe(didpa)(CO)$_2$ (**7**).* Compound **2** (0.150 g, 0.261 mmol) was weighed out in a nitrogen filled MBraun glovebox and added to a Fisher Porter tube. Sodium mercury amalgam (400 mg, 5%Na), a stir bar, and approximately 5 mL of $CH_2Cl_2$ were added to the tube. The tube was closed with a pressure valve and charged with 20 psi of CO and left to stir vigorously overnight. The solvent was then removed using a vacuum, and the solid was redissolved with approximately 10 mL of $Et_2O$. The resultant solution was then filtered through Celite. Slow evaporation of the $Et_2O$ resulted in dark green crystals. Yield: 65% (0.0950 g, 0.170 mmol). FTIR (ATR): 1940, 1872 $cm^{-1}$ (C═O). $^1$H NMR (500 MHz, $CD_2Cl_2$) $\delta$ 8.07 (q, 3H), 7.51 (t, 1H), 7.25 (m, 2H), 4.25 (t, 2H), 3.10 (sep, 2H), 2.88 (t, 2H), 2.73 (s, 3H), 2.51 (sep, 2H), 2.36 (s, 3 H), 1.26 (d, 6 H), 1.05 (d, 18 H). $^{13}$C NMR (500 MHz, $CD_2Cl_2$) expected: 21; reported, 20; $\delta$ 214.9 (C═O), 155.8 ($C_1$−$N_1$), 155.166 ($C_2$−$N_2$), 149.8, 145.8, 140.3, 126.0, 123.2, 120.8, 119.9, 117.2, 62.7, 48.9, 47.8, 27.2, 24.4, 20.0, 20.7, 16.3, 14.3. UV−vis, $CH_2Cl_2$: 368 nm (7472 $cm^{-1}$ $M^{-1}$), 431 nm (9594 $cm^{-1}$ $M^{-1}$), 759 nm (3981 $cm^{-1}$ $M^{-1}$). Anal. calcd for $C_{31}H_{44}O_2FeN_4$: C, 66.42; H, 7.91; N, 9.99. Found: C, 66.32; H, 8.01; N, 9.72.

*[Fe(Hdidpa)(CO)$_2$][PF$_6$] (**8**).* Compound 7 (0.150 g, 0.231 mmol) was dissolved in approximately 5 mL of $CH_2Cl_2$ in a 20 mL scintillation vial. A separate 20 mL scintillation vial was charged with $NH_4PF_6$ (75.2 mg, 0.461 mmol), 3 mL of dry $CH_3OH$, and a stir bar. The reagents were then mixed together and stirred overnight. The solvents were removed via vacuum, and the resulting solid was redissolved in $CH_2Cl_2$. The solution was filtered through Celite to remove any insoluble material. The solvent was removed via vacuum, and the resulting solid was redissolved in $CH_2Cl_2$, layered with ether, and set aside to allow for crystallization. The resulting dark green crystals were washed with ether and dried under vacuum. Yield: 80% (0.130 g, 0.184 mmol). FTIR (ATR): 1946, 1879 $cm^{-1}$ (C═O), 831 $cm^{-1}$ ($PF_6^-$) . $^1$H NMR (500 MHz, $CD_2Cl_2$) $\delta$ 8.18 (br m, 2H), 7.60 (br m, 1H), 7.35 (t, 1H), 7.28 (d, 2H), 4.65 (br m, 2H), 3.82 (br m, 2H), 3.48 (br m, 2H), 2.75 (br s, 3H), 2.51 (m, 5H), 1.51 (d, 12H), 1.27 (m, 6 H), 1.06 (d, 6 H). $^{13}$C NMR (500 MHz, $CD_2Cl_2$) expected: 21, reported, 18; $\delta$ 214.9 (C═O), 158.1 ($C_1$−$N_1$), 156.3 ($C_2$−$N_2$), 149.2, 145.5, 145.1, 140.1, 126.5, 123.6, 122.1, 121.5, 118.5, 48.4, 27.3, 24.4, 23.9, 16.6, 14.5. UV−vis, $CH_2Cl_2$: 354 nm (4489 $cm^{-1}$ $M^{-1}$), 422 nm (6205 $cm^{-1}$ $M^{-1}$), 756 nm (2565 $cm^{-1}$ $M^{-1}$). Anal. calcd for $C_{31}H_{45}F_6O_2FeN_4P$: C, 52.70; H, 6.42; N, 7.93. Found C, 52.01; H, 6.70; N, 7.53. The experimental and theoretical values deviate due to the solvent (methanol) present in the crystals (see Supporting Information).

**$^1$H NMR Titrations.** In a typical experiment, a sample of either [Zn(Hdidpa)Cl$_2$][PF$_6$] (**3**) or [Zn(Hdidpa)Br$_2$][PF$_6$] (**6**) (14 mmol) in $CD_2Cl_2$ (600 $\mu$L) was added to a sealable NMR tube with an injectable screw cap. A hydrogen bond acceptor such as DMF-$d_7$ was titrated in the sealed NMR tube in varying aliquots. The resulting mixture was vigorously shaken for 15 s and inserted into the NMR probe where it was allowed to equilibrate at 298 K for 10 min before a spectrum was obtained. The process was repeated until the titration was complete.

**p*Ka* Determination.** Potentiometric p*K*a titrations were performed in nitromethane and converted to the aqueous scale using the method of Streuli[32] and are the average of three self-consistent trials. Briefly, in a typical experiment, a sample of analyte (0.25 mmol) was placed in a 100 mL volumetric flask. $CH_2Cl_2$ (10 mL) was added to dissolve the analyte, and the flask was filled to mark with nitromethane. A solution of perchloric acid (200 mL, 0.05 M) in nitromethane was used as the titrant. Titrations were performed in a 250 mL beaker using 50 mL aliquots of the solution containing the analyte. Millivolt readings were taken upon delivery of perchloric acid. The end points were determined from derivative plots, and the half neutralization potentials (HNPs) were recorded. Aqueous p*K*a values were determined algebraically within 0.2 p*K*a units using the formula $pK_a(H_2O) = 10.12 - 0.0129 \times \Delta HNP(CH_3NO_2)$, where $\Delta HNP(CH_3NO_2)$ = [HNP(trimethylamine) − HNP(analyte)]. Triethylamine was used as a standard instead of diphenylquanidine.

p*K*a values in acetonitrile were determined by NMR spectroscopy and are the average of three self-consistent trials. In a typical experiment, 11.6 mg (0.0159 mmol) of [Zn(Hdidpa)Cl$_2$][PF$_6$] (**3**) was combined with 1.61 mg (0.0159 mmol) of triethylamine ($pK_a$ = 18.82 in acetonitrile)[33] in an NMR tube and allowed to equilibrate for 60 min. The equilibrium populations were determined by NMR, and the equilibrium concentration was determined from the chemical shift, using the equation $\chi_A = (\delta_{eq} - \delta_B)/(\delta_A - \delta_B)$, where $\chi_A$ is the mole fraction of the conjugate acid, and $\delta$ refers to the measured chemical shift of a given peak at equilibrium (eq) and for pure samples of the conjugate acid (A) and base (B). Once the equilibrium concentrations were obtained, the p*K*a value was calculated utilizing Hess's law.

**Crystallographic Data Collection and Structure Determination.** Diffraction intensities for **1**−**8** were collected at 173(2) K, 200(2) K, and 223(2) K on a Bruker Apex CCD diffractometer using Mo*K*$\alpha$ radiation $\lambda$ = 0.71073 Å or Cu*K*$\alpha$ radiation $\lambda$ = 1.54178 Å. Space groups were determined based on systematic absences. Absorption corrections were applied by SADABS.[34] Structures were solved by direct methods and Fourier techniques and refined on $F^2$ using full matrix least-squares procedures. All non-H atoms were refined with anisotropic thermal parameters. All H atoms in **6** and **8** and H atoms at the N atoms in **3** and **4** involved in N−H···Cl H-bonds were found in the residual density and refined with isotropic thermal parameters. All other H atoms in the investigated structures were refined in calculated positions in a rigid group model. Crystals of **1**, **3**, and **4** were very thin plates, and diffraction intensities at the high angles were very weak. Diffraction at high angles for **2** was weak as well. In all cases, diffraction data were collected up to $2\theta_{max}$ = 56°, but only reflections with $2\theta_{max}$ = 48° (**3**) and 50° (**2**, **4**, and **1**) were involved in the final refinements. Diffraction data for **5** were collected up to $2\theta_{max}$ = 133°, but only reflections with $2\theta_{max}$ = 120° were involved in the final refinements. Even with such restrictions, X-ray diffraction data provide an appropriate ratio of number of measured reflections per refined parameters. The refinement shows that a solvent pentane molecule in **4** and a solvent $OEt_2$ molecule in **5** are disordered around inversion centers. The solvent pentane molecule in **4** is partially occupied in its position; there is 0.25($C_5H_{12}$) per the main cation/anion pair. These disordered solvent molecules were treated by SQUEEZE.[35] The corrections of the X-ray data by SQUEEZE are 51 electron/cell vs the required value of 42 electron/cell in **4** and 85 electron/cell vs the required value of 84 electron/cell in **5**. The Flack parameter in **8** is


DOI: 10.1021/acs.inorgchem.5b00633
*Inorg. Chem.* 2015, 54, 7239−7248

0.008(8). All calculations were performed by the Bruker SHELXTL (v. 6.10) package.[36]

**Mössbauer Spectra.** Mössbauer spectra were recorded at room temperature with a constant-acceleration spectrometer (Wissel GMBH, Germany) in a horizontal transmission mode using a 50 mCi $^{57}$Co source. Approximately 0.080 g of sample was crushed in a Mössbauer sample holder and a drop of Paratone-N was used to cover the sample to prevent oxidation. Data acquisition varied from 2 days to 7 days to get a statistically reasonable spectrum for each sample for analysis. The velocity scale was normalized with respect to a metallic iron at room temperature; hence, all isomer shifts were recorded relative to metallic iron. The Mössbauer spectra were fitted by assuming Lorentzian line shapes using the NORMOS (Wissel GMBH) least-squares fitting program. The isomer shifts and quadrupole splitting parameters were determined from the fitted spectra.

**Computational Methods.** Molecular geometries were optimized and hydrogen bond strengths computed using density functional theory (DFT) within the Perdew–Burke–Ernzerhof (PBE) functional,[37] using the VASP package[38] and projector augmented wave (PAW) potentials.[39] DFT-PBE has been shown to capture hydrogen bond strengths with an error of about 1 kcal/mol.[40] A plane-wave cutoff of 400 eV was used throughout. In each of these calculations, an isolated molecule or ion was placed in a large cubic unit cell, surrounded by approximately 12 Å of vacuum space or more in all directions. Dipole corrections to the total energy were used to account for interactions introduced by periodic boundary conditions.[41]

**Electrochemistry.** Cyclic voltammetry was carried out using a Pine Wavenow potentiostat employing a standard three-electrode electrochemical cell consisting of a glassy carbon working electrode, a platinum auxiliary electrode, and a freshly prepared Ag/Ag$^+$ reference electrode with a vycor tip filled with acetonitrile. All potentials were internally referenced to the ferrocene redox couple. Unless otherwise noted, experiments were carried out under a dinitrogen atmosphere at room temperature using methylene chloride solutions of the analyte at 0.010 M and with 0.100 M tetra(*n*-butyl)ammonium hexafluorophosphate as the supporting electrolyte.

## RESULTS AND DISCUSSION

**Zinc(II) and Iron(II) Didpa Complexes.** The previously reported ligand,[28] [(2,6-$^i$PrC$_6$H$_3$)N=CMe)(N($^i$Pr)$_2$C$_2$H$_4$)N=CMe)C$_5$H$_3$N] (didpa), was utilized to synthesize the zinc(II) and iron(II) derivatives in near quantitative yield (eq 1) by

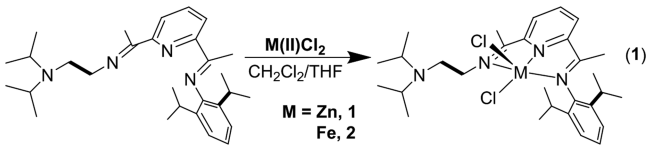


combining the free ligand and either $ZnCl_2$ (**1**) or $FeCl_2$ (**2**) in methylene chloride/THF solution(s). Yellow single crystals of **1** were obtained by layering diethyl ether onto a solution of **1** in methylene chloride and letting stand in a −10 °C freezer for 1 week. Blue single crystals of **2** were obtained by layering pentane onto a solution of **2** in methylene chloride and allowing to stand for 24 h at room temperature. ORTEP views of both **1** and **2** are shown in Figure 2. The Zn(didpa)Br$_2$ complex (**5**) was also synthesized and crystallographically characterized (Table S2, Figure S39, Supporting Information).

Both **1** and **2** are five coordinate with distorted square-pyramidal geometries ($\tau$ = 0.34 for both complexes).[42] In both cases, the nitrogen atoms of the PDI ring along with one chlorine atom make up the basal plane, with the other chlorine atom occupying the apical position. The bond lengths and angles in **1** (Table 1, Figure 2) and **2** (Figure 2) are similar to those of other structurally characterized zinc(II)[43,44] and iron(II)[45−47] complexes containing a PDI ligand. While **1** is diamagnetic in both solution and the solid state, the measured $\mu_{eff}$ of **2** yielded a value of 5.8 $\mu_B$ in the solid state and 5.7 $\mu_B$ in solution, consistent with a high-spin ($S$ = 2) square-pyramidal Fe(II) center.[45] The room temperature, zero-field Mössbauer parameters (Figure S6, Supporting Information) also confirm the assignment of a high-spin Fe(II) center ($\Delta E_Q$ = 1.841(7); $\delta$ = 0.882(3) mm/s).[48−50] In relation to other five coordinate metalloenzyme mimics containing Fe(II)-Cl bonds, the Fe(II)-Cl bond lengths in **2** (2.295(12) and 2.2790(14) Å) are consistent with the Fe(II)-Cl bond lengths found in five coordinate SyrB2 model compounds (2.2653(10) and 2.2646(8) Å, respectively)[51] but shorter than one of the Fe(II)-Cl bond lengths in the recently reported 5-coordinate ($^{Me}$N(afa$^{Cy}$)$_2$)FeCl$_2$ complex. The ($^{Me}$N(afa$^{Cy}$)$_2$)FeCl$_2$ contains two Fe(II)-Cl bonds, one involved in a MHHB and one that is not. The Fe(II)-Cl bond not involved in H-bonding is reported to be 2.309 Å.[52] Lastly, as can be seen from the structural data in Figure 2, all structural metrics (bond lengths and angles) for both **1** and **2** are very similar.

**Secondary Sphere H-Bonding in the Solid State.** In order to probe the secondary coordination sphere H-bonding capabilities of **1** and **2**, the pendant diisopropylamine in each complex was protonated with the weak acid $NH_4PF_6$ (eq 2). This was performed by reaction of either a yellow solution of **1** or a blue solution of **2** in THF with $NH_4PF_6$ in MeOH. These reactions resulted in the formation of the protonated complexes [Zn(Hdidpa)Cl$_2$][PF$_6$] (**3**) and [Fe(Hdidpa)Cl$_2$][PF$_6$] (**4**),

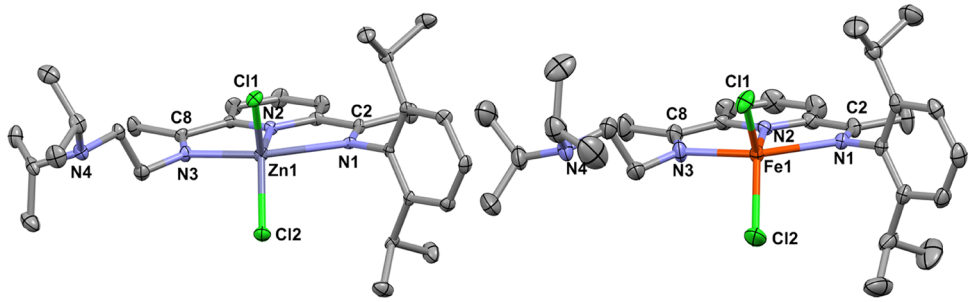


**Figure 2.** Solid-state structures (30% probabilities) of Zn(didpa)Cl$_2$ (**1**) (left) and Fe(didpa)Cl$_2$ (**2**) (right). The H atoms have been omitted for clarity. Selected bond lengths (Å) and angles (deg) for **1**: Zn(1)−Cl(1) 2.251(2), Zn(1)−Cl(2) 2.243(2), Zn(1)−N(1) 2.423(6), Zn(1)−N(2) 2.084(6), Zn(1)−N(3) 2.210(6), C(2)−N(1) 1.278(9), C(8)−N(3) 1.292(9), and Cl(1)Zn(1)Cl(2) 113.89(9), N(2)Zn(1)Cl(1) 127.74(18), and N(1)Zn(1)N(3) 147.9(2). Selected bond lengths (Å) and angles (deg) for **2**: Fe(1)−Cl(1) 2.2959(12), Fe(1)−Cl(2) 2.2790(14), Fe(1)−N(1) 2.285(3), Fe(1)−N(2) 2.117(3), Fe(1)−N(3) 2.192(3), C(2)−N(1) 1.283(5), C(8)−N(3) 1.280(6), and Cl(1)Fe(1)Cl(2) 109.52(6), N(2)Fe(1)Cl(1) 124.58(9), and N(1)Fe(1)N(3) 146.39(13).



DOI: 10.1021/acs.inorgchem.5b00633
*Inorg. Chem.* 2015, 54, 7239−7248

**Table 1. Experimental and DFT-PBE Computed Bond Lengths (Å) and Angles (deg)**

| | 1 | 1 DFT-PBE | 3 | 3 DFT-PBE | 3 DFT-PBE rotated[a] |
|---|---|---|---|---|---|
| Zn(1)−N(2) | 2.084(6) | 2.140 | 2.079(5) | 2.092 | 2.107 |
| Zn(1)−N(3) | 2.210(6) | 2.246 | 2.251(5) | 2.251[b] | 2.251[b] |
| Zn(1)−Cl(2) | 2.243(2) | 2.218 | 2.2346(19) | 2.210 | 2.244 |
| Zn(1)−Cl(1) | 2.251(2) | 2.246 | 2.2696(18) | 2.302 | 2.265 |
| Zn(1)−N(1) | 2.423(6) | 2.446 | 2.240(5) | 2.330 | 2.315 |
| N(1)−C(2) | 1.278(9) | 1.287 | 1.252(8) | 1.290 | 1.290 |
| N(3)−C(8) | 1.292(9) | 1.288 | 1.277(8) | 1.289 | 1.288 |
| C(2)−C(3) | 1.497(10) | 1.496 | 1.488(10) | 1.496 | 1.497 |
| C(7)−C(8) | 1.505(11) | 1.492 | 1.507(9) | 1.497 | 1.499 |
| N(4)-H(1N) | | | 0.99(6) | 1.071 | 1.032 |
| N(4)H(1N)···Cl(1) | | | 2.17(6) | 2.023 | 5.260 |
| N(4)···Cl(1) | | | 3.152(6) | 3.079 | 4.431 |
| N(2)−Zn(1)−Cl(2) | 127.74(18) | 134.01 | 102.51(15) | 129.25 | 133.01 |
| N(2)−Zn(1)−Cl(1) | 118.18(18) | 100.13 | 143.89(15) | 111.93 | 105.96 |
| N(3)−Zn(1)−Cl(1) | 101.91(19) | 100.03 | 97.36(14) | 94.07 | 95.67 |
| Cl(2)−Zn(1)−Cl(1) | 113.89(9) | 125.83 | 113.45(7) | 117.97 | 102.27 |
| N(3)−Zn(1)−N(1) | 147.9(2) | 142.91 | 143.1(2) | 148.34 | 146.12 |
| N(4)-H(1N)-Cl(1) | | | 172(5) | 168.05 | 33.02 |

[a]The N(4)-H(1N) bond was rotated away from Cl(1) and allowed to relax to a relative energy minimum. [b]The Zn(1)−N(3) bond distance was constrained to the experimental value (see text for discussion).

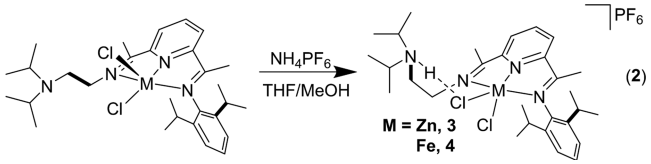


respectively. Layering diethyl ether onto the filtered solution of **3** and letting it stand in a −10 °C freezer for 1 week yielded the yellow crystalline solid **3** in near quantitative yield. Layering pentane into a $CH_2Cl_2$ solution of **4** yielded the purple crystalline solid in yields >90%. ORTEP diagrams of **3** and **4** (the protonated forms of **1** and **2**) are shown in Figure 3. Both metal centers are shifted to an ideal five-coordinate square-pyramidal geometry ($\tau$ = 0.00 for **3** and $\tau$ = 0.06 for **4**). Compound **3** is still diamagnetic in the solid state and solution, whereas the measured $\mu_{eff}$ of **4** yielded a value of 4.7 $\mu_B$ in the solid state and 4.4 $\mu_B$ in solution, consistent with a high-spin ($S$ = 2) square-pyramidal Fe(II) center.[53] The room temperature, zero-field Mössbauer parameters (Figure S11, Supporting Information) also confirm the assignment of a high-spin Fe(II) center ($\Delta E_Q$ = 1.933(8); $\delta$ = 0.863(45) mm/s).[54]

The solid state structures of both **3** and **4** contain M(II)-Cl···H−N MHHBs (M = Zn for **3** and Fe for **4**), which consist of an intramolecular hydrogen bond between the protonated diisopropylamine group and one of the chlorine atoms (the basal Cl atom in **3** and the apical Cl atom in **4**). The hydrogen atom involved in the MHHB was located and refined in both complexes, yielding an N−H···Cl distance of 2.17(6) Å in **3** and 2.18(3) Å in **4**. The N···Cl distances of 3.152(6) Å in **3** and 3.157(8) Å are both consistent with an intramolecular H-bond.[55] The N(4)H(1N) group is directed toward the Cl atom in both compounds, which is also indicative of intramolecular H-bonding;[56]

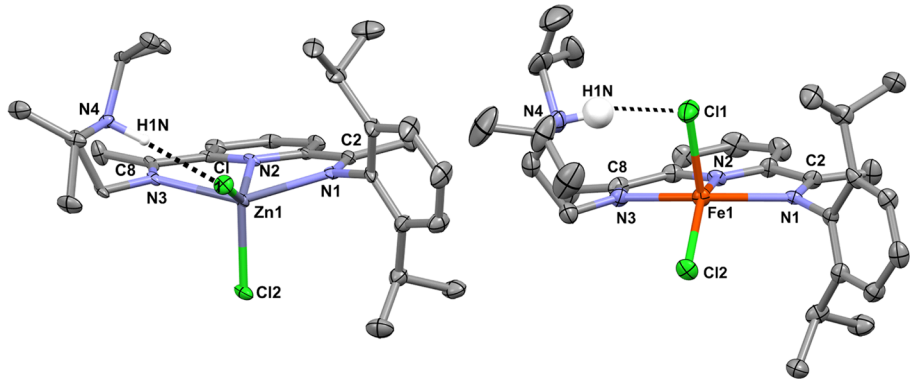


**Figure 3.** Solid-state structures (30% probability) of $[Zn(Hdidpa)Cl_2][PF_6]$ (**3**) (left) and $[Fe(Hdidpa)Cl_2][PF_6]$ (**4**) (right). Only the H atoms involved in H-bonding are shown, and the $PF_6^-$ counterions have been omitted for clarity. H-bonding is denoted by the dashed line. Selected bond lengths (Å) and angles (deg) for **3**: Zn(1)−Cl(1) 2.2696(18), Zn(1)−Cl(2) 2.2346(19), Zn(1)−N(1) 2.240(5), Zn(1)−N(2) 2.079(5), Zn(1)−N(3) 2.251(5), N4-(H1N) 0.99(6), Cl(1)···H(4N) 2.17(6), N(4)···Cl(1) 3.152(6), C(2)−N(1) 1.252(8), C(8)−N(3) 1.277(8), and Cl(1) Zn(1)Cl(2) 113.45(7), N(2) Zn(1)Cl(1) 143.89(15), N(1) Zn(1)N(3) 143.1(2), and N(4)-H(1N)···Cl(1) 172(5). Selected bond lengths (Å) and angles (deg) for **4**: Fe(1)−Cl(1) 2.327(2), Fe(1)−Cl(2) 2.263(2), Fe(1)−N(1) 2.225(6), Fe(1)−N(2) 2.102(5), Fe(1)−N(3) 2.215(7), N4-(H4N) 1.00(2), Cl(1)···H(4N) 2.18(3), N(4)···Cl(1) 3.157(8), C(2)−N(1) 1.282(8), C(8)−N(3) 1.283(9), and Cl(1)Fe(1)Cl(2) 111.94(9), N(2)Fe(1)Cl(2) 142.54(17), N(1)Fe(1)N(3) 146.1(2), and N(4)-H(4N)···Cl(1) 166(10).



DOI: 10.1021/acs.inorgchem.5b00633
*Inorg. Chem.* 2015, 54, 7239−7248

the N−H···Cl angle is 172(5)° in **3** and 166(10)° in **4**. The discrepancy in the N−H···Cl angle in the two compounds may be due to the different $Cl^-$ ligand (one basal and one apical) involved in each MHHB. In both cases, the $\nu_{N-H}$ in the solid state infrared spectrum is obscured (absent) by H-bonding.[57] There are peaks in the IR spectra at ∼2690 $cm^{-1}$ (see the Supporting Information), which fall in the range of $R_3NH^+$ complexes.[58] However, isotopic substitution experiments with $ND_4PF_6$ as the $D^+$ source were inconclusive.

Neither M(II)-Cl bond in each complex involved in the MHHB is appreciably elongated. The Zn(II)-Cl bond distance is 2.251(2) Å in **1** and 2.2696(18) Å in **3**. A very slight elongation of the Fe(II)-Cl bond from 2.2959(12) Å in **2** to 2.327(2) Å in **4** is observed, which may or may not be due to the MHHB. As stated above, the Fe(II)-Cl bond length in five-coordinate SyrB2 model complexes[51] (which do not display any MHHBs) are 2.26 Å, shorter than the Fe(II)-Cl bond in **4**. The formation of an intramolecular H-bond in the secondary coordination sphere MHHB between the protonated pendant base arm and the halide ligand was also observed in the solid state structure of our previously reported $[Fe(Hdidpa)Br_2][PF_6]$.[28] Elongation of the Fe(II)-Br bond involved in the secondary coordination sphere MHHB was also attenuated. The Fe(II)-Br bond distance in $[Fe(Hdidpa)Br_2][PF_6]$ was found to be 2.4439(6) Å and 2.4252(4) Å in $Fe(didpa)Br_2$. For comparison, the Fe(II)-Cl bond involved in MHHB in the 5-coordinate $(^{Me}N(afa^{Cy})_2)FeCl_2$ complex[52] is elongated from 2.309 to 2.420 Å.

$[Zn(Hdidpa)Br_2][PF_6]$ (**6**) was also synthesized and crystallographically characterized (Table S2, Figure S40, Supporting Information). Similar to **3**, the solid state structure of **6** contains an intramolecular Zn(II)-Br···H−N MHHB between the protonated diisopropylamine group and the basal bromine atom. In relation to complex **3**, the N−H···Br and N···Br distances are elongated (2.45(4) and 3.309(3) Å, respectively) in **6**, with the N−H···Br angle of 174(3)°, suggesting a weaker MHHB interaction with the bromide as compared to the chloride.[55]

**Secondary Sphere H-Bonding in Solution.** Given that the $\nu_{N-H}$ peaks in the solid-state IR spectra of **3** and **4** are absent due to hydrogen bonding (and that the paramagnetic nature of the Fe(II) center prevents analysis by NMR), it was not possible to investigate the nature of the secondary coordination sphere MHHB interaction of the iron complexes in solution (i.e., H-bond conservation, strength, etc.). Because of the inherent structural similarities between the zinc(II) and the iron(II) complexes, we performed a set of experiments on the diamagnetic **1** and **3** to probe the nature of the MHHB in solution.

With **1** in hand, the p*K*a of the pendant diisopropylamine in didpa was determined in both aqueous and acetonitrile solutions (see Supporting Information). The aqueous values (which were collected in nitromethane and then converted to the aqueous scale)[32] were found to be 10.4 in the free ligand and 9.7 once the didpa ligand is bound to $ZnCl_2$ in **1**. These values compare favorably to those of free Hünigs base (diisopropylethylamine), which has a reported p*K*a of 10.8 in aqueous solution.[59] In acetonitrile, the pendant diisopropylamine of **1** has a measured p*K*a of 18.4, compared to the measured value for Hünigs base of 18.8. What is clear from these data is that the basicity of the pendant diisopropylamine is not attenuated appreciably once the ligand is bound to the zinc ion. This is likely due to the ethylene bridge electronically insulating the base from the metal (as opposed to an aryl bridge). In similar systems that contain arylphosphine ligands tethered with pendant bases, the p*K*a values of the pendant groups are severely attenuated once the phosphine is bound to a transition metal ion.[60] For example, the reported dimethylamine appended triphenylphosphine has a p*K*a of 18.0 when free and 13.0 when bound to a rhenium(I) center. This suggests that the base is able to communicate electronically through the aryl group, leading to severe attenuation in the p*K*a values, which is not observed in our systems.

In the case of **3** and **6**, which are diamagnetic in both the solid state and solution, diagnostic $^1H$ NMR spectra can be obtained, and the $^1H$ NMR spectra of **3** in $CD_2Cl_2$ are shown in Figure 4. The N−H resonance of **3** is shifted downfield to 8.50 ppm, suggesting significant deshielding of the proton environment. This observation is consistent with an H-bond interaction in solution between the protonated amine of the didpa ligand and the chloride bound to the zinc.[11,14,15,61] The same effect is seen in the $^1H$ NMR spectrum of **6**, where the N−H resonance is

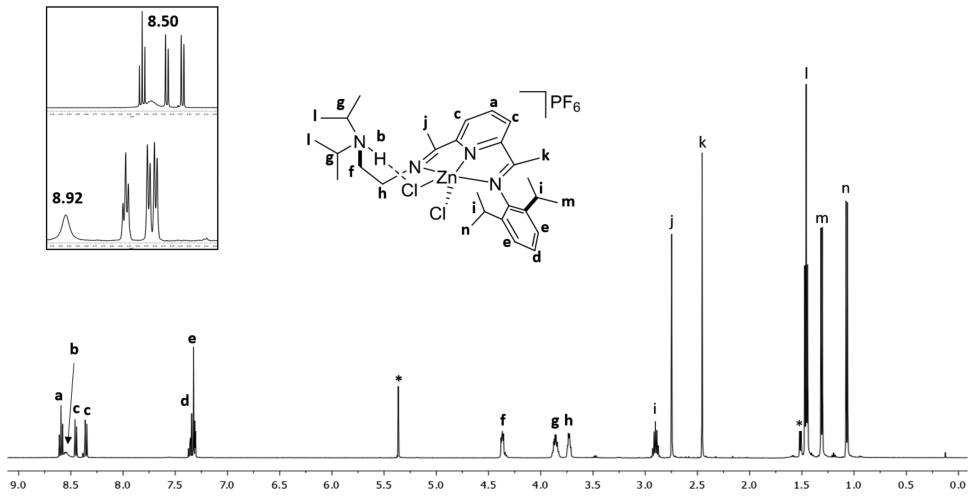


**Figure 4.** $^1H$ NMR spectrum of $[Zn(Hdidpa)Cl_2][PF_6]$ (**3**) in $CD_2Cl_2$ at 298 K. The inset shows the N−H resonance in $CD_2Cl_2$ before (top) and after the addition of 50 equiv of DMF-$d_7$ (bottom). The * represents solvent.



DOI: 10.1021/acs.inorgchem.5b00633
*Inorg. Chem.* 2015, 54, 7239−7248

shifted downfield to 7.79 ppm, suggesting a weaker MHHB in solution (Figure S16, Supporting Information).

In order to probe the relative strength of the N−H···Cl H-bond in **3** in solution, the N−H resonance was interrogated via a series of $^1$H NMR titrations with solvents of differing $\beta$ values (thermodynamic measure of H-bonding acceptance ability).[62] If intermolecular H-bonding to bulk solvent is possible, then the N−H resonance in the $^1$H NMR spectrum should undergo a downfield shift when increasing amounts of hydrogen bond acceptor are added. Accordingly, when deuterated solvents of different H-bond accepting strength (acetone < DMF < DMSO) were titrated into a $CD_2Cl_2$ solution of **3** (Figure 5), drastically different downfield shifts

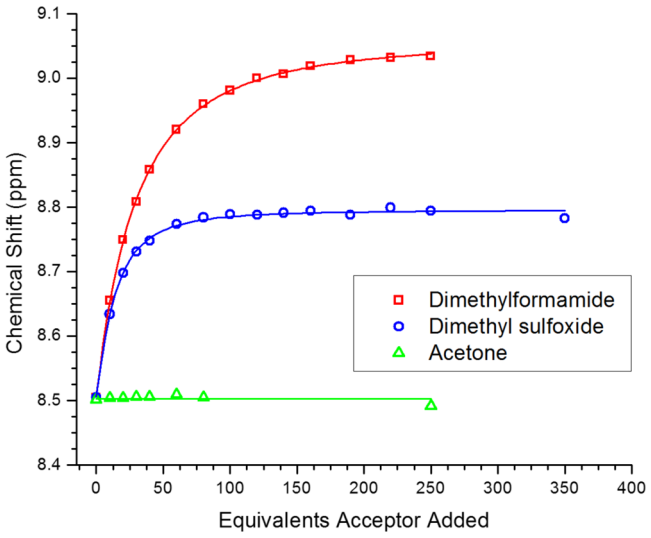


**Figure 5.** Binding isotherms of the titration of the hydrogen bond acceptors acetone-$d_6$ (green triangle), DMSO-$d_6$ (blue circle), and DMF-$d_7$ (red square) with **3**. Plot of chemical shift of the N−H resonance vs equivalents of the H-bond acceptor added.

were observed for the different solvents. Addition of up to 250 equiv with acetone-$d_6$ ($\beta$ = 0.43) resulted in no downfield shift of the N−H resonance, consistent with no H-bonding interaction with acetone. However, addition of the stronger H-bond accepting solvents DMF-$d_7$ ($\beta$ = 0.69) and DMSO-$d_6$ ($\beta$ = 0.76) resulted in a downfield shift of the N−H resonance from 8.50 to 9.04 and 8.78 ppm, respectively, and more importantly, a change in the shape of the binding isotherms (Figure 5). Each spectrum was internally referenced to TMS, and the shift in the N−H resonance was significantly larger than that for any other resonance in the spectrum. It should be noted that nonspecific changes in the chemical shift can occur due to changes in the solvent dielectric over the course of the titration. However, the small shifts in the non-N−H resonances (~0.05 ppm) indicate that the changes in the solvent dielectric are small compared to the shift in the N−H resonance (~0.3 ppm for DMSO-$d_6$ and ~0.5 ppm for DMF-$d_7$). From the binding isotherms in Figure 5, values of the association constants were extracted utilizing an iterative fitting program[63] that correlated with a weak association with the H-bond accepting solvent ($K_{DMF}$ = 1.1 L mol$^{-1}$ and $K_{DMSO}$ = 2.4 L mol$^{-1}$). These data suggest that in poor H-bond accepting solvents like methylene chloride and acetone, the Zn(II)-Cl···H−N *intra*molecular interaction is more favorable than an *inter*molecular H-bonding interaction with external solvent. When the H-bond acceptance value of the solvent is increased, the intermolecular H-bonding interaction is favored. An identical trend is observed in the case of the binding isotherms when **3** is replaced with **6** (Figure S37, Supporting Information). The association constants of **6** with the H-bonding solvent observed ($K_{ACETONE}$ = 0.01 L mol$^{-1}$, $K_{DMF}$ = 4.8 L mol$^{-1}$, and $K_{DMSO}$ = 8.1 L mol$^{-1}$) in the case of **6** are larger due to the weaker Zn(II)-Br···H−N intramolecular interaction (compared to Zn(II)-Cl···H−N).[55]

**H-Bond Strength Computations.** To obtain a more quantitative value for the H-bond strength in **3**, we computed the hydrogen bond strength by comparing the total energy of the hydrogen-bonded cation (Figure 6, left) to a hypothetical cation in which the N(4)-H(1N) bond was rotated away from the chloride ligands (Figure 6, right). The latter structure was determined by adding a proton to the structure of **1** (assuming that is the conformation that minimizes steric repulsion) and computationally relaxing it. The Zn(1)−N(3) bond was constrained to the experimental value of 2.251 Å in this treatment due to an overestimation of the computed Zn(1)−N(3) bond length of 2.523 Å when unconstrained (Supporting Information). This elongation of the Zn(1)−N(3) bond length resulted from an additional interaction between N(3) and H(1N) when unconstrained (the N(3) ···H(1N) distance was computed as 2.648 Å when unconstrained, whereas the N(3)···H(1N) distance in the crystal structure of **3** was found to be 2.839 Å). By this method, the hydrogen bond strength of the N(4)-H(1N)···Cl(1) interaction in **3** was found to be 5.9 kcal/mol.

As can be seen from Table 1, the computed bond lengths complement the experimental values found from the X-ray crystal structure. All bond lengths fall within 2% of the experimental values. The computed bond angles deviate somewhat from experiment, which is to be expected, as deviations of

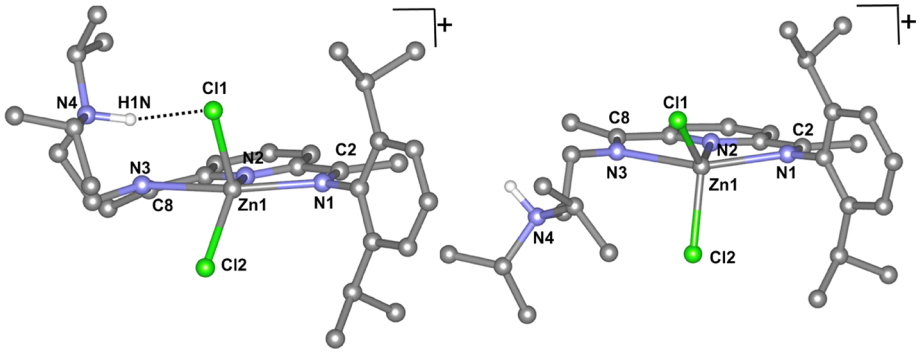


**Figure 6.** DFT-PBE computed structures of [Zn(Hdidpa)Cl$_2$]$^+$ (**3 DFT-PBE**) (left) and [Zn(Hdidpa)Cl$_2$]$^+$ (**3 DFT-PBE rotated**) (right). In **3 DFT-PBE rotated**, the protonated pendant base has been rotated away from the chloride ligands. The H-bond is denoted by the dashed line.



DOI: 10.1021/acs.inorgchem.5b00633
*Inorg. Chem.* 2015, 54, 7239−7248

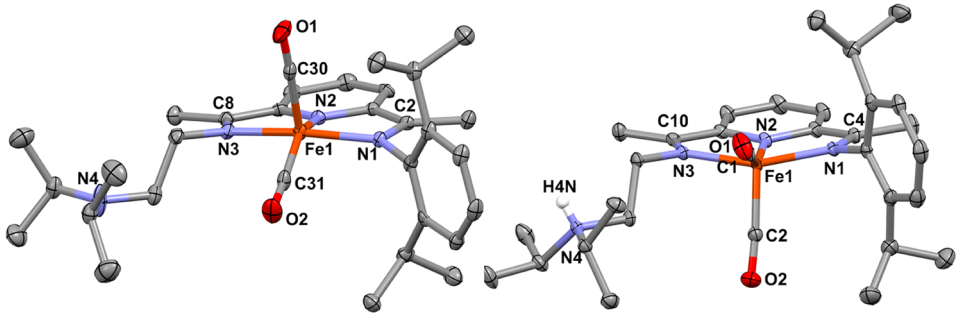


**Figure 7.** Solid-state structure (30% probability) of $Fe(didpa)CO_2$ (**7**) (left) and $[Fe(Hdidpa)(CO)_2][PF_6]$ (**8**) (right). Only the H atom of the protonated diisopropylamine is shown, and the $PF_6^-$ counterion has been omitted for clarity. Selected bond lengths (Å) and angles (deg) for **7**: Fe(1)−C(31) 1.774(6), Fe(1)−C(30) 1.788(7), Fe(1)−N(1) 1.961(5), Fe(1)−N(2) 1.846(4), Fe(1)−N(3) 1.960(5), C(2)−N(1) 1.330(7), C(8)−N(3) 1.329(7), and C(31)Fe(1)C(30) 98.9(3), N(2)Fe(1)C(31) 149.2(3), and N(1)Fe(1)N(3) 156.99(19). Selected bond lengths (Å) and angles (deg) for **8**: Fe(1)−C(1) 1.779(2), Fe(1)−C(2) 1.7821(18), Fe(1)−N(1) 1.9617(15), Fe(1)−N(2) 1.8452(15), Fe(1)−N(3) 1.9461(16), N4-(H4N) 0.74(3), C(4)−N(1) 1.317(2), C(10)−N(3) 1.329(3), and C(1)Fe(1)C(2) 94.29(9), N(2)Fe(1)C(1) 151.19(8), and N(1)Fe(1)N(3) 154.70(6).

similar magnitude have been observed for **DFT-PBE** calculations of molecules and molecular crystals[64] (especially in proximity to hydrogen bonds)[40] due to their relatively flat potential energy surfaces. For comparison, the analogous N−H···X-M H-bond strengths of the protonated $[Zn(Hdidpa)Br_2]^+$ (4.9 kcal/mol) and $[Zn(Hdidpa)I_2]^+$ (3.8 kcal/mol) complexes were also computed (see Supporting Information). The data are in excellent qualitative agreement with the observed trend in N−H···X-M H-bond strengths, where N−H···Cl-M > N−H···Br-M > N−H···I-M.[55] Lastly, the computed N−H···Cl value of 5.9 kcal/mol in **3** is consistent with other recently published H···Cl-M bond strengths.[8,65]

**pH Coupled Ligand-Based Redox Activity.** Metalloenzymes are recognized for their propensity to tune the redox state(s) of the active site(s), as well as the protonation state of the surrounding residues in the secondary coordination sphere.[1,16] In order to probe the synergy between the redox activity and the protonation state of the didpa scaffold, **2** was reduced under a CO atmosphere with NaHg amalgam producing the doubly reduced $Fe(didpa)(CO)_2$ complex, **7**. The ORTEP diagram of the diamagnetic green complex (**7**) is shown in Figure 7 (left). The iron center is five coordinate, square pyramidal ($\tau = 0.12$). The $C_{imine}$-$N_{imine}$ bonds are elongated from a value of 1.283(5) and 1.280(6) Å in **2** to 1.3330(7) and 1.329(7) Å. The $C_{imine}$−$C_{ipso}$ bonds are contracted from 1.489(6) and 1.491(6) Å in **2** to 1.433(8) and 1.430(8) Å. These data, taken in conjunction with the zero-field Mössbauer parameters ($\Delta E_Q = 1.43$, $\delta = -0.06$ mm/s), suggest that complex **7** is best described as an iron(II) center with a doubly reduced didpa ligand (Figure S21, Supporting Information). Previous reports by us,[29,66] and others,[67] have suggested that iron compounds in the doubly reduced PDI to be in the diradical dianionic form.[68] The FTIR spectrum of **7** displays two $\nu_{CO}$ values at 1940 and 1871 $cm^{-1}$, respectively, in the range of $FePDI(CO)_2$ complexes best described as having diradical dianionic ligands with a S = 0 Fe(II) center.[67] Inspection of the p*K*a (acetonitrile) of the pendant base reveals a value of 19.2. This value is similar (albeit higher) to the $Zn(didpa)Cl_2$ compound (18.4) and free Hünigs base (18.8). The increase in the observed p*K*a value could be attributed to the ligand being more electron rich in the doubly reduced state. Regardless, the ethylene bridge prevents wild deviation in the p*K*a of the pendant base, similar to that of other systems where the acidic/basic sites are separated from the redox active sites of the complex.[19]

Reaction of **7** with $NH_4PF_6$ produces the protonated, reduced complex $[Fe(Hdidpa)(CO)_2][PF6]$, **8**. The ORTEP diagram of the diamagnetic green complex (**8**) is also shown in Figure 7 (right). The iron center is five coordinate, square pyramidal ($\tau = 0.06$). The $C_{imine}$−$N_{imine}$ bonds are 1.317(2) and 1.329(3) Å, whereas the $C_{imine}$−$C_{ipso}$ are 1.430(3) and 1.431(3) Å, suggesting no change in the oxidation state upon protonation of the didpa scaffold. The zero-field Mössbauer parameters ($\Delta E_Q = 1.435(8)$, $\delta = -0.075(5)$ mm/s) confirm this observation (Figure S25, Supporting Information). The FTIR spectrum of **8** displays two $\nu_{CO}$ at 1946 and 1879 $cm^{-1}$, respectively. These values are shifted to slightly higher wavenumber from **7**, suggesting less electron density at the Fe(II) center upon protonation of pendant diisopropylamine.[69]

To investigate how the protonation state of the ligand affects the redox-active sites in the scaffold, we examined the cyclic voltammetry of both **7** and **8** in $CH_2Cl_2$. Previous work[29,66,70] has shown that the PDI ligand scaffold in $FePDI(CO)_2$ complexes is capable of undergoing a reversible (or quasi-reversible) one electron oxidation to form $[FePDI(CO)_2]^+$, where the redox-active ligand is involved in the electron transfer (not the metal center, eq 3).

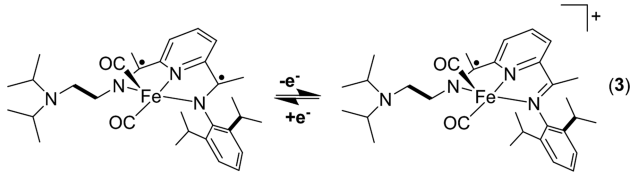


As seen in Figure 8, in $CH_2Cl_2$ both complexes **7** and **8** undergo the quasi-reversible one electron oxidation of the didpa ligand scaffold, albeit at different potentials.[71] For the neutral form, **7**, the oxidation of the ligand occurs at $E_{1/2} = -0.590$ V. Upon protonation to **8**, the event occurs at $E_{1/2} = -0.485$ V. The ligand becomes more difficult to oxidize upon protonation, which is to be expected, but only a modest 105 mV shift in potential is observed. For comparison, an approximate shift of ∼500 mV in potential is observed for transition metal complexes upon protonation/deprotonation of a ligand bound directly to the metal center.[72,73] In other systems where the protonation site and redox active site are separated, the


DOI: 10.1021/acs.inorgchem.5b00633
*Inorg. Chem.* 2015, 54, 7239−7248

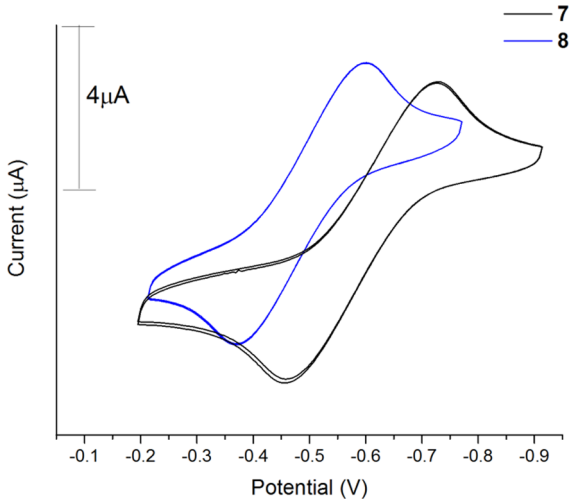


**Figure 8.** CV of 0.005 M Fe(didpa)$CO_2$ (**7**) (black line) and 0.010 M $[Fe(Hdidpa)(CO)_2][PF_6]$ (**8**) (blue line); 0.1 M $[(^nBu)_4N][PF_6]$ in $CH_2Cl_2$, 200 mV/s scan rate, glassy carbon working electrode, 2 repeat scans shown, internally referenced to ferrocene. Scans were started at −0.7 V running anodically.

redox and acid/base chemistry are still strongly coupled. For example, the tetraphenylporphyrin (TPP) 4-methylimidazole (ImH) derivatives $[(TPP)Fe^{II}(ImH)_2]$ and $[(TPP)Fe^{III}(ImH)_2][PF_6]$ have $E_{IM} = -0.95$ V and $E_{IMH} = -0.585$ V for the $Fe^{III/II}$ couple in the protonated (IMH) and unprotonated (IM) 4-methylimidazole ligand.[19] A similar effect is seen in the well explored $Fe^{II}$(tris(2,2′biimdazoline)$^{2+}$ ($Fe^{II}H_2$bim) and $Fe^{II}$(tris(2,2′-tetyrahydropyrimidine)$^{2+}$ ($Fe^{II}H_2$bip) systems.[72] Lastly, H-bonding ligands have also been invoked as a method to tune the redox potential of metal centers.[65,74] One explanation as to why the redox activity in the systems compared above is more pronounced than in **7** and **8** is that those redox events are metal-centered. In **7** and **8**, the redox events are *ligand-centered*. In both **7** and **8**, the electronics at the iron center seem to be insulated from the protonation state of the ligand, as judged by the slight shift (~6 $cm^{-1}$) in the FTIR spectrum and virtually no shift in the Mössbauer spectra. However, the one electron oxidation/reduction of the ligand scaffold is clearly affected by the pH state of the pendant base.

## CONCLUSIONS

In summary, we have synthesized and characterized a series of zinc(II) and iron(II) complexes based on the pyridinediimine core. These complexes contain a pendant diisopropylamine capable of forming secondary coordination sphere MHHBs upon protonation with the weak acid, $NH_4PF_6$. The p*K*a (acetonitrile) of the pendant diisopropylamine group was found to be 18.4 in the zinc complex, $Zn(didpa)Cl_2$, which showed that the basicity of the pendant group was not attenuated once the free ligand was coordinated to the metal ion. The solution behavior of the MHHBs was probed via $^1$H NMR titrations of $[Zn(Hdidpa)Cl_2][PF_6]$ and $[Zn(Hdidpa)Br_2][PF_6]$ with solvents of varying H-bond accepting strength. The H-bond strength in $[Zn(Hdidpa)Cl_2][PF_6]$ and $[Zn(Hdidpa)Br_2][PF_6]$ was calculated *in silico* to be 5.9 and 4.9 kcal/mol, respectively. The intimacy of the secondary coordination sphere acidic/basic sites and the ligand-based redox-active sites were probed through the synthesis and characterization of $Fe(didpa)(CO)_2$ and $[Fe(Hdidpa)(CO)_2][PF_6]$. The p*K*a (acetonitrile) of the pendant diisopropylamine group was found to be 19.2 in $Fe(didpa)(CO)_2$. The electronics of the metal center are only modestly affected by changing the protonation state of the ligand, whereas the ligand-based redox-activity is coupled to the pH of the ligand.

## ASSOCIATED CONTENT

### Supporting Information

X-ray crystallographic data, Mössbauer spectra, spectroscopic data, CIF files, titration data, and DFT-PBE computed structures of $[Zn(Hdidpa)Br_2]^+$ and $[Zn(Hdidpa)I_2]^+$. The Supporting Information is available free of charge on the ACS Publications website at DOI: 10.1021/acs.inorgchem.5b00633.

## AUTHOR INFORMATION

### Corresponding Author

*E-mail: gilbertson@chem.wwu.edu.

### Notes

The authors declare no competing financial interest.

## ACKNOWLEDGMENTS

This research was supported by a CAREER award from the National Science Foundation (CHE-1255570) and an award from the ACS PRF (53427-UR3). We thank Yubin Kwon for assistance with magnetic susceptibility experiments.

## REFERENCES

(1) Borovik, A. S. *Acc. Chem. Res.* **2005**, *38*, 54−61.
(2) Lu, Y.; Valentine, J. S. *Curr. Opin. Struct. Biol.* **1997**, *7*, 495−500.
(3) Holm, R. H.; Kennepohl, P.; Solomon, E. I. *Chem. Rev.* **1996**, *96*, 2239−2314.
(4) Berreau, L. M. *Eur. J. Inorg. Chem.* **2006**, *2006*, 273−283.
(5) Jeffery, G. A.; Saenger, W. *Hydrogen Bonding in Biological Structures*; Springer-Verlag: Berlin, Germany, 1991.
(6) Rosenthal, J.; Nocera, D. G. *Acc. Chem. Res.* **2007**, *40*, 543−553.
(7) Rakowski DuBois, M.; DuBois, D. L. *Chem. Soc. Rev.* **2009**, *38*, 62−72.
(8) Moore, C. M.; Quist, D. A.; Kampf, J. W.; Szymczak, N. K. *Inorg. Chem.* **2014**, *53*, 3278−3280.
(9) Hart, J. S.; Nichol, G. S.; Love, J. B. *Dalton Trans.* **2012**, *41*, 5785−5788.
(10) Hart, J. S.; White, F. J.; Love, J. B. *Chem. Commun.* **2011**, *47*, 5711−5713.
(11) Sickerman, N. S.; Park, Y. J.; Ng, G. K. Y.; Bates, J. E.; Hilkert, M.; Ziller, J. W.; Furche, F.; Borovik, A. S. *Dalton Trans.* **2012**, *41*, 4358−4364.
(12) Park, Y. J.; Sickerman, N. S.; Ziller, J. W.; Borovik, A. S. *Chem. Commun.* **2010**, *46*, 2584−2586.
(13) Matson, E. M.; Bertke, J. A.; Fout, A. R. *Inorg. Chem.* **2014**, *53*, 4450−4458.
(14) Mareques Rivas, J. C.; de Rosales, R. T. M.; Parsons, S. *Dalton Trans.* **2003**, 2156−2163.
(15) Mareques Rivas, J. C.; Salvagni, E.; de Rosales, R. T. M.; Parsons, S. *Dalton Trans.* **2003**, 3339−3349.
(16) Warren, J. J.; Mayer, J. M. *Biochemistry* **2015**, DOI: 10.1021/acs.biochem.5b00025.
(17) Proton-Coupled Electron Transfer Themed Issue. *Chem. Rev.* **2010**, *110*, 6937− 7100.
(18) Dempsey, J. L.; Winkler, J. R.; Gray, H. B. *Chem. Rev.* **2010**, *110*, 7024−7039.
(19) Warren, J. J.; Mayer, J. M. *J. Am. Chem. Soc.* **2008**, *130*, 2774−2776.
(20) Manner, V. W.; Mayer, J. M. *J. Am. Chem. Soc.* **2009**, *131*, 9874−9875.
(21) DuBois, D. L.; Bullock, R. M. *Eur. J. Inorg. Chem.* **2011**, *2011*, 1017−1027.


DOI: 10.1021/acs.inorgchem.5b00633
*Inorg. Chem.* 2015, 54, 7239−7248

(22) Helm, M. L.; Stewart, M. P.; Bullock, R. M.; DuBois, M. R.; DuBois, D. L. *Science* **2011**, *333*, 863−866.
(23) Wiese, S.; Kilgore, U. J.; Ho, M.-H.; Raugei, S.; DuBois, D. L.; Bullock, R. M.; Helm, M. L. *ACS Catal.* **2013**, *3*, 2527−2535.
(24) Yang, J. Y.; Bullock, R. M.; Shaw, W. J.; Twamley, B.; Fraze, K.; DuBois, M. R.; DuBois, D. L. *J. Am. Chem. Soc.* **2009**, *131*, 5935−5945.
(25) Chirik, P. J. *Inorg. Chem.* **2011**, *50*, 9737−9740.
(26) Luca, O. R.; Crabtree, R. H. *Chem. Soc. Rev.* **2013**, *42*, 1440−1459.
(27) Lyaskovskyy, V.; de Bruin, B. *ACS Catal.* **2012**, *2*, 270−279.
(28) Kendall, A. J.; Zakharov, L. N.; Gilbertson, J. D. *Inorg. Chem.* **2010**, *49*, 8656−8658.
(29) Thammavongsy, Z.; LeDoux, M. E.; Breuhaus-Alvarez, A. G.; Seda, T.; Gilbertson, J. D. *Eur. J. Inorg. Chem.* **2013**, *2013*, 4008−4015.
(30) Sur, S. K. *J. Magn. Reson.* **1988**, *82*, 169−173.
(31) Bain, G. A.; Berry, J. F. *J. Chem. Educ.* **2008**, *85*, 532−536.
(32) Streuli, C. A. *Anal. Chem.* **1959**, *31*, 1652−1654.
(33) Kaljurand, I.; Kutt, A.; Soovali, L.; Rodima, T.; Maemets, V.; Leito, I.; Koppel, I. A. *J. Org. Chem.* **2005**, *70*, 1019−1028.
(34) Sheldrick, G. M. *Bruker/Siemens Area Detector Absorption Correction Program*; Bruker AXS: Madison, WI, 1998.
(35) Van der Sluis, P.; Spek, A. L. *Acta Crystallogr., Sect. A: Found. Crystallogr.* **1990**, *46*, 194−201.
(36) *SHELXTL-6.10, Program for Structure Solution, Refinement and Presentation*; BRUKER AXS Inc.: Madison, WI.
(37) Perdew, J. P.; Burke, K.; Ernzerhof, M. *Phys. Rev. Lett.* **1996**, *77*, 3865−3868.
(38) Kresse, G.; Furthmüller, J. *Phys. Rev. B: Condens. Matter Mater. Phys.* **1996**, *54*, 11169−11186.
(39) Kresse, G.; Joubert, D. *Phys. Rev. B: Condens. Matter Mater. Phys.* **1999**, *59*, 1758−1775.
(40) Ireta, J.; Neugebauer, J.; Scheffler, M. *J. Phys. Chem. A* **2004**, *108*, 5692−5698.
(41) Makov, G.; Payne, M. C. *Phys. Rev. B: Condens. Matter Mater. Phys.* **1995**, *51*, 4014−4022.
(42) A $\tau$ value of 1 corresponds to an ideal trigonal bipyramidal geometry, whereas a $\tau$ value of 0 corresponds to an ideal square pyramidal geometry. See: Addison, A. W.; Rao, T. N.; Reedjik, J.; van Rijn, J.; Verschoor, G. C. *J. Chem. Soc., Dalton Trans.* **1984**, 1349−1356.
(43) Fan, R. Q.; Zhu, D. S.; Ding, H.; Mu, Y.; Su, Q.; Xia, H. *Synth. Met.* **2005**, *149*, 135−141.
(44) Edwards, D. A.; Mahon, M. M.; Martin, W. R.; Molloy, K. C.; Fanwick, P. E.; Walton, R. A. *J. Chem. Soc., Dalton Trans.* **1990**, 3161−3168.
(45) Small, B. L.; Brookhart, M.; Bennett, A. M. A. *J. Am. Chem. Soc.* **1998**, *120*, 4049−4050.
(46) Britovsek, G. J. P.; Bruce, M.; Gibson, V. C.; Kimberley, B. S.; Maddox, P. J.; Mastroianni, S.; McTavish, S. J.; Redshaw, C.; Solan, G. A.; Strömberg, S.; White, A. J. P.; Williams, D. J. *J. Am. Chem. Soc.* **1999**, *121*, 8728−8740.
(47) Bianchini, C.; Mantovani, G.; Meli, A.; Migliacci, F.; Zanobini, F.; Laschi, F.; Sommazzi, A. *Eur. J. Inorg. Chem.* **2003**, *2003*, 1620−1631.
(48) Bart, S. C.; Chlopek, K.; Bill, E.; Bouwkamp, M. W.; Lobkovsky, E.; Neese, F.; Wieghardt, K.; Chirik, P. J. *J. Am. Chem. Soc.* **2006**, *128*, 13901−13912.
(49) Enright, D.; Gambarotta, S.; Yap, G. P. A.; Budzelaar, P. H. M. *Angew. Chem., Int. Ed.* **2002**, *41*, 3873−3876.
(50) Britovsek, G. J.; Clentsmith, G. K. B.; Gibson, V. C.; Goodgame, D. M. L.; McTavish, S. J.; Pankhurst, Q. A. *Catal. Commun.* **2002**, *3*, 207−211.
(51) Friese, S. J.; Kucera, B. E.; Young, V. G.; Que, L., Jr.; Tolman, W. B. *Inorg. Chem.* **2008**, *47*, 1324−1331.
(52) Matson, E. M.; Gordon, Z.; Lin, B.; Nilqes, M. J.; Fout, A. R. *Dalton Trans.* **2014**, *43*, 16992−16995.
(53) The discrepancy in the magnetic moment between **2** and **4** is likely due to a change in geometry as well as the protonation state. Both complexes are well within the range of a high spin Fe(II) center.
(54) The RT Mössbauer spectrum of **4** revealed a small iron containing impurity at 0.6 mm/s, likely due to the oxidation of **4** during data acquisition.
(55) Brammer, L.; Bruton, E. A.; Sherwood, P. *Cryst. Growth Des.* **2001**, *1*, 277−290.
(56) Luck, W. A. P. In *The Hydrogen Bond: Recent Developments in Theory and Experiments*; Schuster, P., Zundel, G., Sandorfy, C., Eds.; North-Holland: New York, 1976; pp 527− 562.
(57) Steiner, T. *Angew. Chem., Int. Ed.* **2002**, *41*, 48−76.
(58) Pasto, D. J.; Johnson, C. R. *Organic Structure Determination*; Prentice Hall: Englewood Cliffs, NJ, 1969; p 121.
(59) Perrin, D. D. *Dissociation Constants of Organic Acids and Bases*; Butterworths: London, 1965. Supplement 1972.
(60) Teets, T. S.; Labinger, J. A.; Bercaw, J. E. *Organometallics* **2013**, *32*, 5530−5545.
(61) Berreau, L. M.; Makowska, M. M.; Arif, A. M. *Inorg. Chem.* **2001**, *40*, 2212−2213.
(62) Marcus, Y. *Chem. Soc. Rev.* **1993**, *22*, 409−416.
(63) Bisson, A. P.; Hunter, C. A.; Morales, J. C.; Young, K. *Chem. - Eur. J.* **1998**, *4*, 845−851.
(64) Bucko, T.; Hafner, J.; Lebegue, S.; Angyan, J. G. *J. Phys. Chem. A* **2010**, *114*, 11814−11824.
(65) Mareque Rivas, J. C.; Hinchley, S. L.; Metteau, L.; Parsons, S. *Dalton Trans.* **2006**, 2316−2322.
(66) Thammavongsy, Z.; Seda, T.; Zakharov, L. N.; Kaminsky, W.; Gilbertson, J. D. *Inorg. Chem.* **2012**, *51*, 9168−9170.
(67) Computational studies on Fe(*i*PrPDI)$(CO)_2$ show that an $Fe^0$, $d^8$ electronic description may be acceptable. Therefore, the electronic structure may be a hybrid of the $Fe^0$ and $Fe^{II}$ resonance forms. See also: Stieber, S. C. E.; Milsmann, C.; Hoyt, J. M.; Turner, Z. R.; Finkelstein, K. D.; Wieghardt, K.; DeBeer, S.; Chirik, P. J. *Inorg. Chem.* **2012**, *51*, 3770−3785.
(68) Bart, S. C.; Chlopek, K.; Bill, E.; Bouwkamp, M. W.; Lobkovsky, E.; Neese, F.; Wieghardt, K.; Chirik, P. J. *J. Am. Chem. Soc.* **2006**, *128*, 13901−13912.
(69) The protonated diisopropyalamine group is involved in H-bonding to a MeOH solvent molecule in the solid state, where the N(4)-H(4N)···O(1S)#1 was 2.821(2) Å and the N(4)H(4N)O(1S) angle = 174(2)°. See Supporting Information.
(70) Tondreau, A. M.; Milsmann, C.; Lobkovsky, E.; Chirik, P. J. *Inorg. Chem.* **2011**, *50*, 9888−9895.
(71) Linear plots of $i_p$ vs the square root of the scan rate are shown in the Supporting Information.
(72) Warren, J. J.; Tronic, T. A.; Mayer, J. M. *Chem. Rev.* **2010**, *110*, 6961−7001.
(73) Weinberg, D. R.; Gagliardi, C. J.; Hull, J. F.; Fecenko Murphy, C.; Kent, C. A.; Westlake, B. C.; Paul, A.; Ess, D. H.; Granville McCafferty, D.; Thomas J. Meyer, T. J. *Chem. Rev.* **2012**, *112*, 4016−4093.
(74) Natale, D.; Mareque-Rivas, J. C. *Chem. Commun.* **2008**, 425−437.


DOI: 10.1021/acs.inorgchem.5b00633
*Inorg. Chem.* 2015, 54, 7239−7248